Scholars Journal of Engineering and Technology

OPEN ACCESS

Abbreviated Key Title: Sch J Eng Tech
ISSN 2347-9523 (Print) | ISSN 2321-435X (Online)
Journal homepage: https://saspublishers.com

Dynamic Evolution of the Slag Phases During the Foaming Practice in the BOF Converter

Elena Brandaleze[1]*, Marcelo Alejandro Valentini[1], Leandro Matías Santini[1], Edgardo Roque Benavidez[1]

[1]Metallurgy Department, Universidad Tecnológica Nacional-Facultad Regional San Nicolás, Colón 332, San Nicolás, 2900, Buenos Aires, Argentina

DOI: https://doi.org/10.36347/sjet.2026.v14i06.004 | **Received:** 26.04.2026 | **Accepted:** 10.06.2026 | **Published:** 12.06.2026

***Corresponding author:** Elena Brandaleze
Metallurgy Department, Universidad Tecnológica Nacional-Facultad Regional San Nicolás, Colón 332, San Nicolás, 2900, Buenos Aires, Argentina

Abstract | **Original Research Article**

Various operational practices are currently employed in steelmaking to extend the service life of BOF converter refractory linings. Consequently, understanding interface behavior within the slag-refractory system is crucial for assessing how evolving slag phases impact lining protection. Since slag foaming effectively shields the refractory up to the trunnion zone, it is essential to gather data on the dynamic evolution of these phases and their influence on physical properties under operational conditions. Surface-active species present in the slag affect foam stability. Thermodynamic simulations using FactSage 8.1 provide key insights into the evolution of solid and liquid phases during foaming. When correlated with physical properties, such as viscosity, surface tension, and foaming index values derived from experimental techniques and theoretical calculations, these results offer a robust approximation of operational conditions. This paper also includes comprehensive pre- and post-foaming structural characterization using optical microscopy and scanning electron microscopy (SEM+EDS) carried out on samples from different foaming stages. The information obtained provides a deeper understanding of slag evolution during refractory protection practices, enabling the improvement of foam behavior and efficiency.

Keywords: Interface, Microstructure, Physical property, Slag, Thermodynamic simulation.

INTRODUCTION

The application of slag foaming practice in oxygen converters (BOF) plays a relevant role to protect MgO-C refractory lining life (Martinsson *et al.,* 2019). Slag dynamic behaviour depends on the phases evolution, because determine the foam character (Jung & Fruehan, 2000). Slag behaviour changes during operation are controlled by the chemical composition and process conditions. The slag viscosity behaviour and gas amount contained significantly affect the foaming process and the foaming index. For this reason, the main objective of this paper is focused on a study of the slag phases and structure evolution in correlation with the (slag) chemical composition during the foaming practice. This information allows us to understand the foaming micro mechanisms in direct relation with the present phases characteristics in the system. Foaming height is influenced by the basicity index (IB), the oxide composition, and the degree of slag polymerization (Wang *et al.,* 2023). The stability and height of slag foam are governed by the liquid film drainage of slag bubbles, which can lead to bubble coalescence and foam collapse. Additionally, the FeO content in molten slag significantly affects its physical properties (Brandaleze E. *et al.,* (2018). During the BOF conversion process, the FeO in the molten slag reacts with the carbon in the steel, as shown in the equation (1):

$$(FeO)+[C]=[Fe] + CO(g) \qquad (1)$$

The steel decarburization reaction promotes slag foaming in the BOF. An adequate slag foaming protects refractory lining life and provides good conditions for the chemical reactions and energy efficiency in the converter. However, a slag foaming excess could produce slopping risk. Therefore, for security in the industrial operations it is necessary to carry out a good control of slag foaming height during the practice.

Slag foam is constituted by a gas/liquid emulsion, with a lower liquid volume than gas. To predict foaming behavior, it is important to know the slag physical properties, such as viscosity and surface tension, both of which are influenced by the dynamic evolution of slag phases. Surface tension increases with

basicity index rise and temperature decrease. Foam life is greater at higher viscosity and lower surface tension. The foam decay is caused by the elimination of the liquid films in the bubbles by drainage (Brandaleze E. *et al.,* 2018). Higher viscosity values promote lower film drainage rate in the bubbles (Skupien D. & Gaskell D. R., 2000). This study investigates the structural phases of multicomponent BOF slag samples collected under pre- and post-foaming conditions to elucidate the relationship between slag physical properties, foam behavior, and the melt microstructure. Various experimental techniques, such as optical and scanning electron microscopy (SEM+EDS), were employed for slag characterization. In addition, the dynamic evolution of these systems was predicted using FactSage thermodynamic simulations to complement the structural evolution study. The converter slag system comprises a complex mixture of oxides, primarily SiO2, CaO, FeOx, MgO, and P2O5. The oxide SiO2 forms a polymeric network of $[SiO4]4-$ tetrahedra. Si atoms are bridged to O atoms by Si-O bonds, forming a three-dimensional network structure. Specific oxides present, such as MgO, CaO, and FeO, are considered modifiers as they promote the rupture of Si-O bonds (depolymerization), resulting in an increase of non-bridging oxygen atoms. This phenomenon decreases the degree of slag polymerization.

Slag foaming phenomena were initially studied under steady-state conditions. However, it is crucial to consider that the reactions involved in these processes are associated with changes in slag chemical composition and gas formation rates, both of which fluctuate during operation, creating dynamic conditions. Furthermore, slag composition evolves continuously due to reactions between the slag and lining dissolution products (Kapilashrami A., *et al.,* 2006). For this reason, the slag characterization results obtained from pre- and post-foaming samples were integrated with thermodynamic simulations under non-equilibrium conditions. The slag foam height was estimated using the foaming index (Σ), according to expression (2) reported by Fruehan and Matsuura (Matsuura and Fruehan, 2009).

$$\Sigma = 115\frac{\mu^{1/2}}{\sigma^{0.2}\rho D_B^{0.9}} \quad (2)$$

Where: DB, μ, ρ, αvδ σ are the foam bubble diameter, slag viscosity, slag density and slag surface tension, respectively.

In this study, two models (Urbain G., 1982) and (Zaharia *et al.,* 2009) were used to determine viscosity and surface tension values, respectively; to establish the foaming index. The results were completed with information obtained by the thermal behavior of the slags determined by hot stage microscopy (HSM). In the silicate melts, surface tension impact on foaming depends on the active component's concentration, present in the surface slag bubble films and on the thermodynamic activity of the solute in the melt. The main surface-active component consists in Si-O- anions bonds which are oriented toward the bulk with negative charge. These anions are compensated with cations present in the slag film. In agreement with (Skupien D. & Gaskell D. R., 2000), the surface layer is a bipolar one and presents a high viscosity which promotes foam stability.

Gas bubble size in the slag determines foaming behavior. Foam with small bubbles is dense and minimizes the risk of converter slopping while promoting better slag adherence to the refractory surface. In contrast, large soap-like bubbles generate foam instability, increasing the possibility of slopping. Two types of foam can be distinguished: (i) foams initially formed by spherical bubbles separated by thick liquid films, and (ii) polyhedral foams, in which bubbles are deformed due to liquid film drainage. This drainage phenomenon reduces the thickness of the separating liquid film to values lower than 1μm (Brandaleze *et al.,* 2018).

Computational modeling has become a vital tool for advancing pyrometallurgical knowledge, enabling significant improvements in industrial design and operations. Specifically, thermodynamic slag simulation offers rapid insights to address BOF-related challenges (Zaaiman S. *et al.,* 2024). Building on this, the present paper provides key findings regarding slag foaming behavior derived from these models.

MATERIAL AND METHODS

In this study, BOF slag samples were collected at two distinct process stages: (a) pre-foaming (Samples A) and (b) post-foaming (Samples D). Their chemical compositions are detailed in Table 1.

Table1. Chemical composition of the converter (BOF) slags samples (%wt.)

Sample	% SiO_2	% CaO	% Al_2O_3	% MgO	% FeO	% MnO	% P_2O_5	% S
1A	12.7	50.0	1.50	5.90	27.8	4.90	3.05	0.15
1D	12.3	52.5	1.76	5.47	23.4	4.46	2.50	0.14
2A	14.9	41.4	1.79	9.34	31.4	5.32	1.71	0.056
2D	14.9	43.9	2.04	7.85	30.2	5.15	1.69	0.089
3A	17.7	43.5	1.66	5.45	27.6	3.78	1.28	0.058
3D	16.7	47.5	1.85	6.98	25.6	3.90	1.32	0.085

The slag samples were characterized including theoretical calculus and experimental assays. The binary basicity index values (IB2=CaO/SiO2) were calculated based on the chemical composition of the samples. Additionally, the determination of physical properties, specifically viscosity (η), surface tension (γ), and foaming index (Σ), was conducted by applying various theoretical models. Viscosity values were determined using the Urbain model (Urbain G. ,1982), while surface tension values were calculated according to the model proposed by Zaharia *et al.,* (Zaharia *et al.,* 2009). The melting behavior of the slags was experimentally determined using hot stage microscopy (HSM). Subsequently, the foaming index (Σ) was calculated via equation (2), considering two distinct bubble diameters (D1=0.005 m and D2=0.015 m).

To obtain information on the slag structural phases characteristics and composition, the slag samples were prepared for the microscopy observation. All the samples studied by microscopy technique were mounted in a conductive resin and polished with SiC papers (180-1000). Then they were mechanically polished using a diamond suspension from 9 µm to 1 µm, followed by vibratory polishing using 0.05 µm alumina. The structural study was performed by light microscopy using an Olympus GX51 microscope applying with Material Plus image analysis system and scanning electron microscopy (SEM) including EDS (semiquantitative) analysis, using a FEI Quanta 200 instrument.

To analyze the phase evolution of the slag systems during BOF foaming, thermodynamic simulations were performed using FactSage 8.1. The methodology employed non-equilibrium conditions based on the Scheil-Gulliver cooling model (Durinck *et al.,* 2007). The FToxid, FTsalt, and FactPS (version 8.1) databases were used, covering a temperature range from 1650°C down to 300°C.

RESULTS AND DISCUSSION

This study investigates foaming behavior in BOF slags during the first half of the blowing period to identify key variables and slopping risks. Additionally, samples were collected post-foaming to better understand slag evolution throughout the converter process.

Slags samples PROPERTIES

Comparing the chemical compositions of pre- and post-foaming slag (Samples A and D, respectively) reveals significant variations in oxide levels during the BOF operation. As shown in (Figure 1), the most notable changes across the three sample sets involve their CaO and FeO contents.

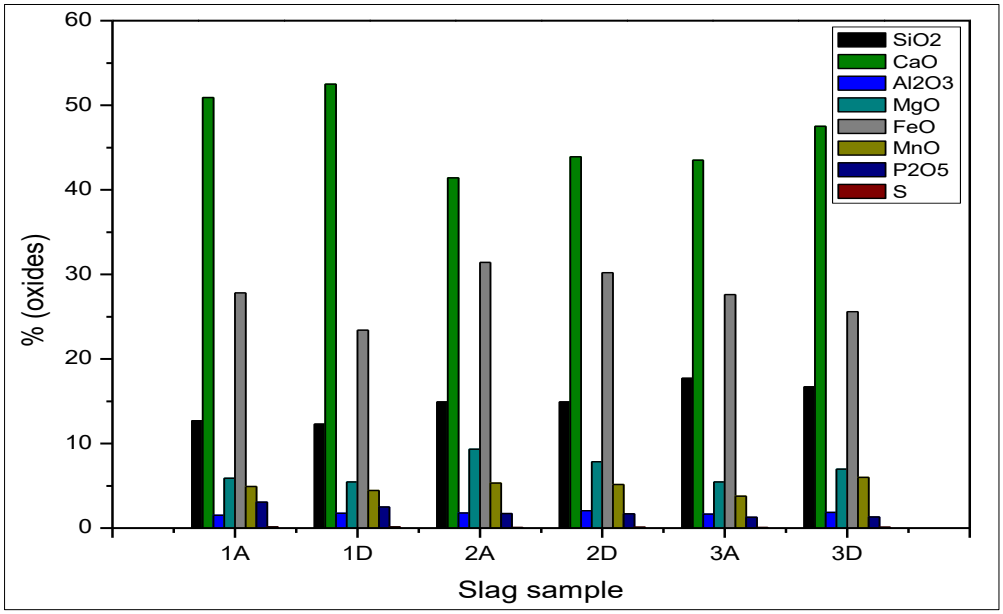

Figure 1: Comparison between slags chemical compositions in pre- and post-foaming stages (A and D, respectively)

Slag properties estimated from chemical composition include binary basicity index (IB2 = CaO/SiO2) and surface tension (γ) at 1650°C (BOF process temperature). The results obtained are detailed in (Table 2).

In the CaO–SiO2–FeO system at 1400 °C, S decreased as basicity rose to 1.22. However, when the CaO/SiO2 ratio exceeded 1.22, S increased due to the presence of second-phase particles, such as CaO or 2CaOSiO2 (Jung and Fruehan, 2000).

In all the slag samples (A and D), IB2 values are higher than 1.22. This suggests that, under the studied conditions, BOF slags contain significant quantities of second-phase particles that promote foaming behavior. Slags 1A and 1D, which exhibit higher IB2 values, contain more CaO and less SiO2 than the other slags, and

they also show the highest γ values. These findings align with (Sukenaga S. *et al.,* 2015).

Table 2: Binary basicity index (IB_2) and surface tension (γ) values of the slag samples

Sample	IB_2	γ (mN/m)
1A	3.94	652
1D	4.27	644
2A	2.76	625
2D	2.95	628
3A	2.46	615
3D	2.84	624

Variations in g values are driven by the local structure of the slag at the melt surface. While oxygen atoms in the bulk are fully coordinated with cations, those at the surface often lose neighboring bonds. This creates "unsatisfied" or dangling bonds, the higher the density of these bonds, the greater the surface tension.

According to the results informed by (Liu, C. et al.,2021), the increasing of IB2 ratio form 0.5 to 2.0 (such as the IB2 values of slags A and D), promotes the progressive depolymerization of [SiO4] and [PO4] tetrahedra by O2- ions. Simultaneously, Ca2+ stabilizes [FeO4] units, facilitating the structural transition from [FeO6] octahedra to [FeO4] tetrahedra. Although this enhances the network-forming role of Fe3+, the overall count of non-bridging oxygens (NBOs) increases. Consequently, the higher density of NBOs in the surface layer, characterized by higher unsatisfied energy, results in an increase in surface tension. The slags A and D with higher g values also present the higher contents of P2O5 in the chemical composition. Consequently, these phenomena underpin the values exhibited by the slag systems under investigation. In converter slags, Si4+, Fe3+ and P5+ are all potential network-formers. Their simultaneous presence can induce non-linear variations in physical properties as a function of composition, a phenomenon known as the "mixed network-forming effect".

The Urbain model (Urbain, 1982) was employed to predict the temperature-dependent viscosity of the slags, as illustrated in Figure 2. The results indicate that slag viscosity decreases as basicity increases across all studied samples. This physical property also is controlled by the slag's structural factors and the FeO content. It is known that viscosity of slag increases as FeO content decreases (Brandaleze *et al.,* 2018).

The melting behavior and critical temperatures of the slags were determined via hot-stage microscopy (HSM). Figure 3 presents the average values for softening (Ts), hemisphere (Th), and fluidity (Tf) temperatures. The observed increase in critical temperatures for Samples D, relative to Samples A, is attributed to the evolution of chemical composition and phase transitions occurring during the BOF process.

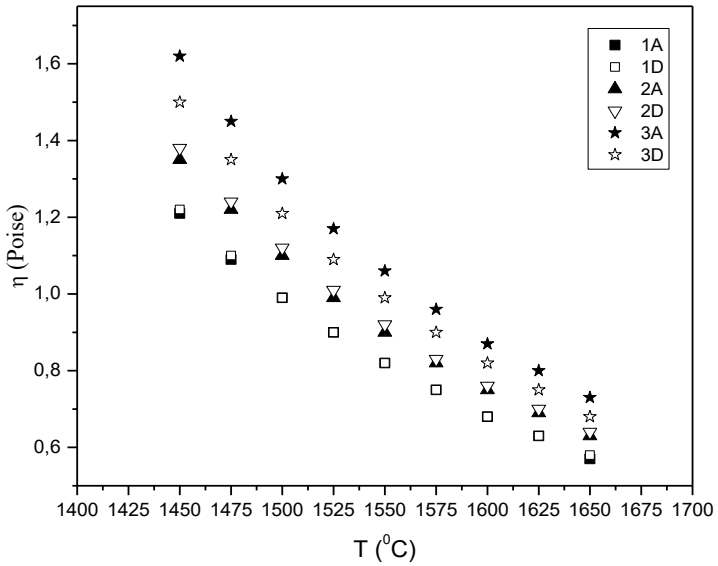

Figure 2: Viscosity behaviour of the six slags samples in relation with temperature

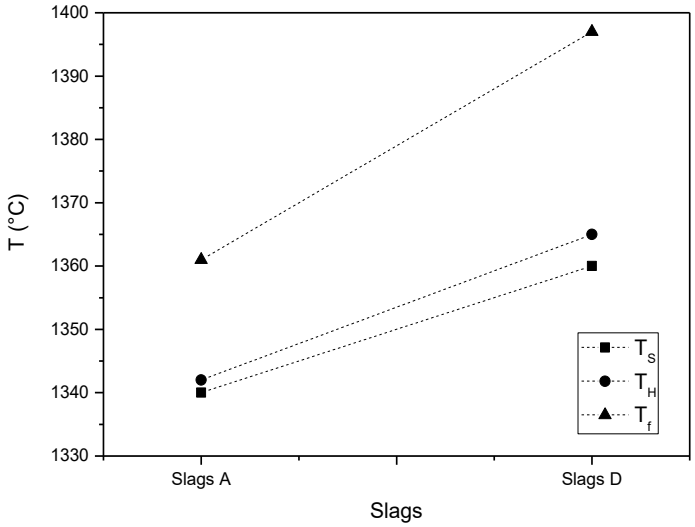

Figure 3: Average critical temperatures values of the slag samples (A and D)

The foaming index values (Σ) for the slag samples was determined for two distinct bubble diameters (D1 = 0.005 m and D2 = 0.015 m), using the expression (2) (Matsura H. & Fruehan R.J., 2009). The results are summarized in Table 3. Samples 1 (A and D) exhibited the lowest values for both diameters. These samples are further characterized by the highest basicity (IB2) and surface tension (γ), alongside the lowest viscosity at 1600 °C compared to the other slags.

Table 3: Foaming index values (Σ) of the slag samples calculated for two bubbles diameters values

Sample	Σ (D_1 = 0.005 m)	Σ (D_2 = 0.015 m)
1A	0.193	0.072
1D	0.199	0.074
2A	0.212	0.079
2D	0.218	0.081
3A	0.265	0.098
3D	0.247	0.092

BOF slags are complex systems, constituted by heterogeneous mixtures of solid, liquid, and gaseous phases. The properties evolution suggest that slag systems undergo different phases changes during foaming, which could explain the behavioral differences observed between samples. The presence of solid dicalcium silicate particles (Ca2SiO4) has been verified to enhance foaming stability. These precipitates act as stabilizers at the gas-liquid interface, significantly increasing the effective foaming index S.

SLAGS STRUCTURE AND PHASES CHARACTERIZATION

The microstructure of BOF slag samples (A and D) was examined via optical microscopy to evaluate phase transformations occurring before and after the foaming practice. Structural comparisons are illustrated in Figures 4a–4f. All samples exhibit significant variations in phase types, morphologies, and their relative proportions.

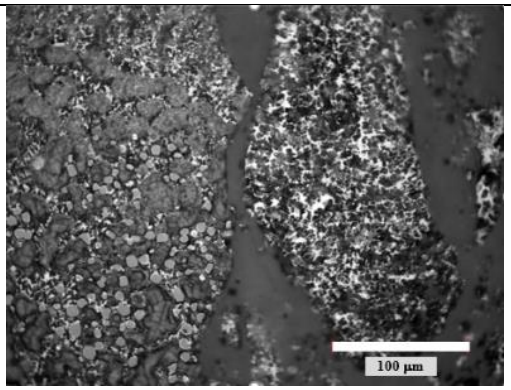

(a) Phases observed in slag 1A

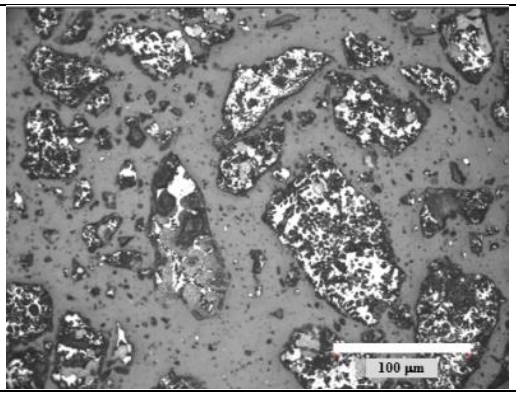

(b) Phases observed in the slag 1D

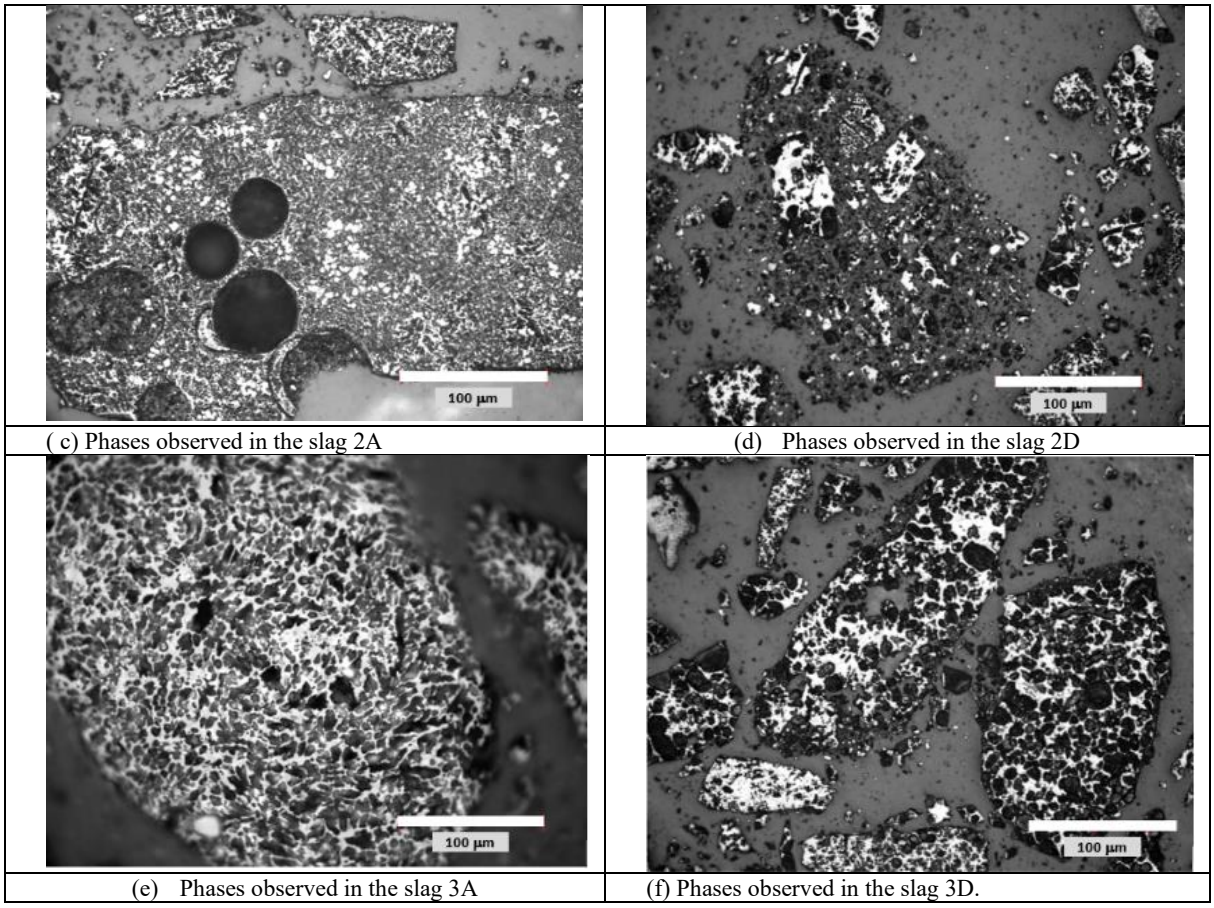

(c) Phases observed in the slag 2A | (d) Phases observed in the slag 2D

(e) Phases observed in the slag 3A | (f) Phases observed in the slag 3D.

Figure 4: Comparative analysis of phase evolution and microstructural features in slag samples

Spherical pores were observed within the microstructure of slag sample 2A. The microstructural features and primary phases of the slag samples were analyzed using Scanning Electron Microscopy (SEM) and Energy Dispersive Spectroscopy (EDS). The phases identified in Samples 1A and 1D (which exhibit the highest basicity (IB2), highest surface tension (g), and lowest viscosity (h)) differ significantly from those observed in Samples 3A and 3D, which display contrasting physical properties. Pre-foaming slag sample 1A exhibits a complex microstructure with diverse phase morphologies, as initially observed via light microscopy. Detailed SEM analysis at higher magnification identified the primary phases as: (a) polygonal (P), (b) dendritic (R), (c) irregular grey (FG), and (d) irregular white (FW) phases. These are all dispersed within a continuous grey matrix (M), as illustrated in (Figure 5). Post-foaming slag sample 1D also exhibits a diverse mineralogical structure: (a) a laminar phase (L) containing entrapped steel droplets, (b) an irregular phase (I), and (c) an irregular phase (FP). All identified phases are dispersed within a continuous matrix (M), as shown in Figure 6.

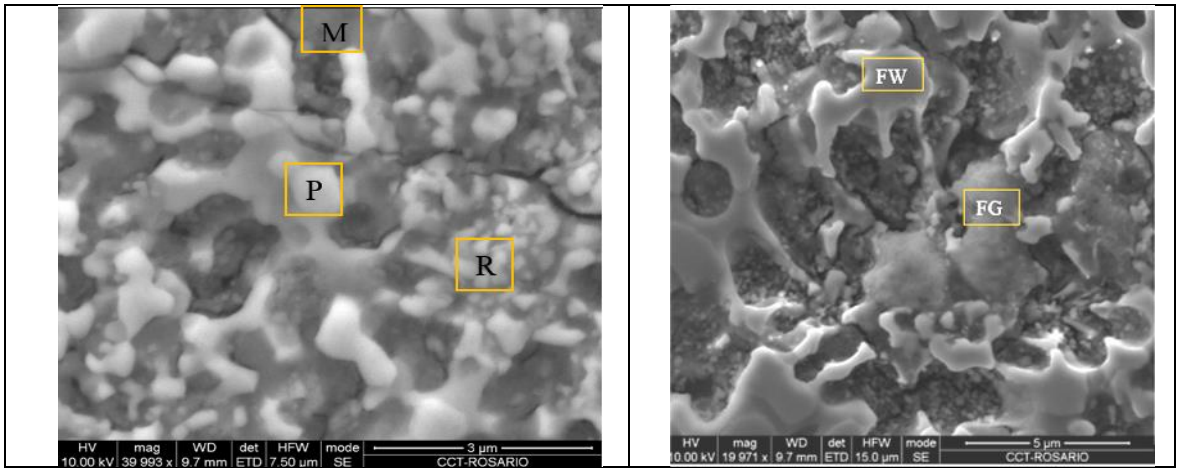

Figure 5: Slag phases identified in the sample 1A

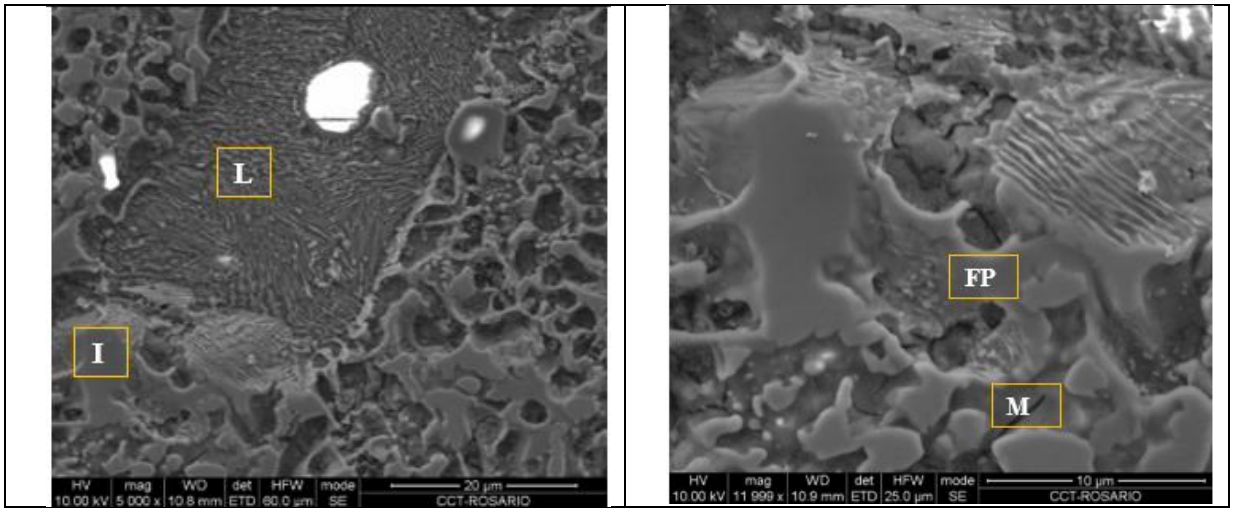

Figure 6: Slag phases identified in the sample 1D

The slags 1A and 1D phases chemical composition were determined by semiquantitative EDS analysis. The oxides contents are Figure 7 (a) and (b).

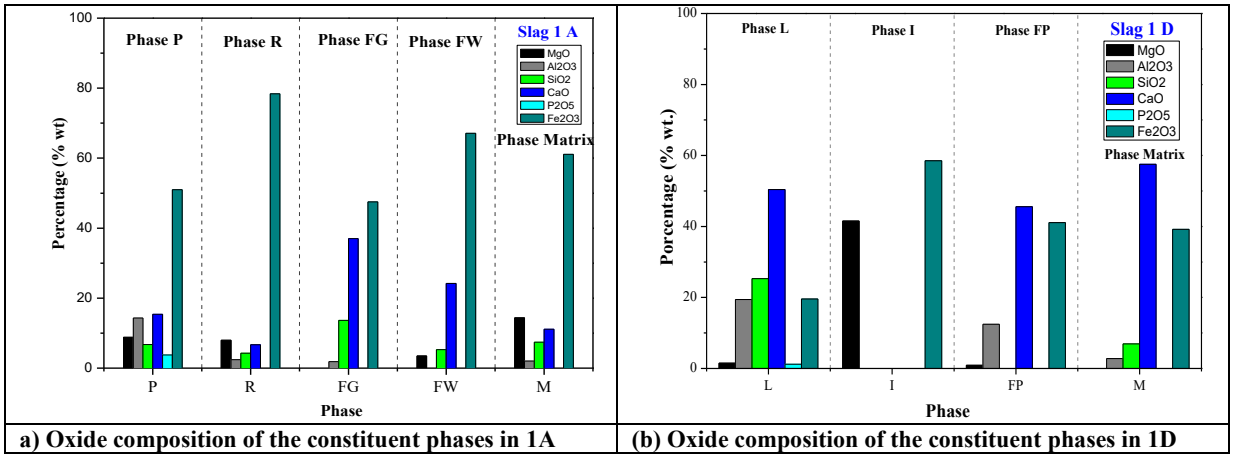

a) Oxide composition of the constituent phases in 1A **(b) Oxide composition of the constituent phases in 1D**

Figure 7: Oxide composition of the constituent phases in slag 1A and 1D

The mineralogical phases in Samples 3A and 3D exhibit distinct chemical compositions and morphological characteristics that differ significantly from the other slag samples. Figure 8 illustrates the granular morphology of the matrix phase (M) in Sample 3A, which is consistent with the observations in Sample 3D. This granular texture is distinct from the other slag samples studied. In these samples, the matrix phase (M) coexists within a complex mixture with the (SAC) phase. Furthermore, the irregular phase (I) contains embedded polygonal crystals, identified as the (MW) phase.

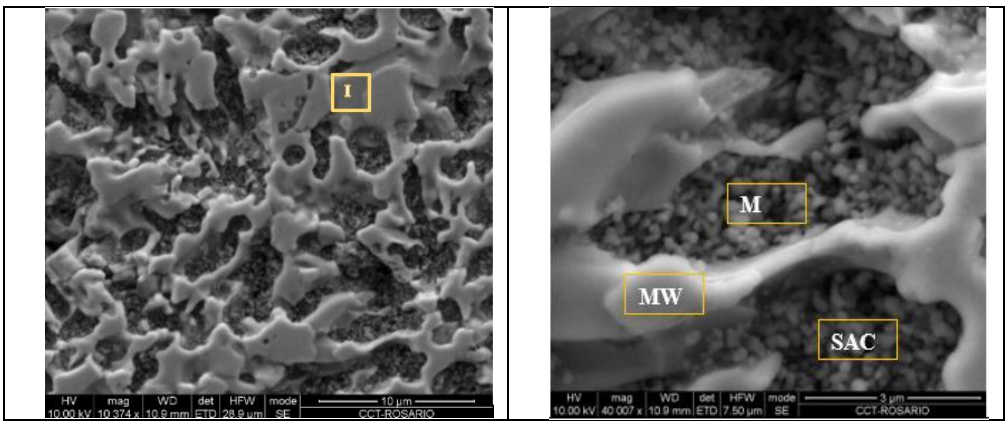

Figure 8: Phases identified in the slag sample 3A

The chemical compositions of the phases in Samples 3A and 3D, as determined by EDS, are remarkably similar. They are presented together in Figure 9.

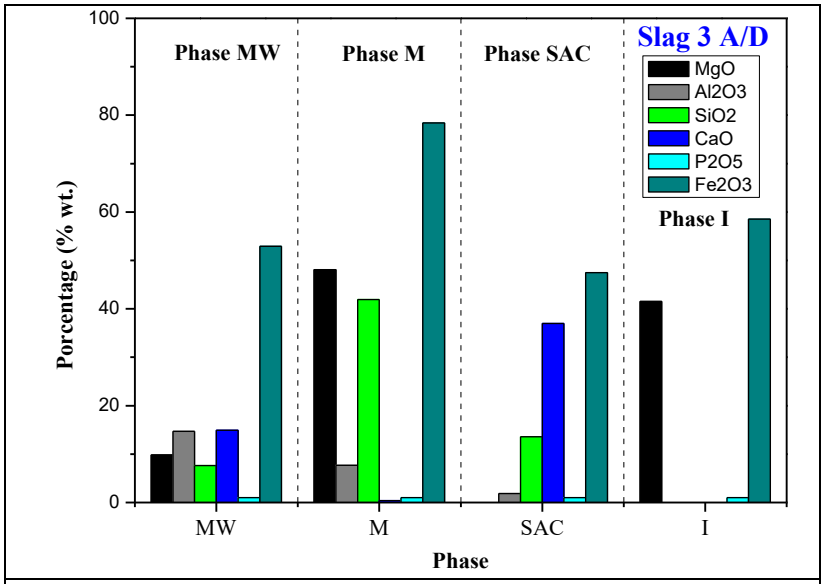

Figure 9: Oxide composition of the constituent phases in 3 A/D

THERMODYNAMIC SIMULATION OF THE SLAGS PHASES EVOLUTION

In this study, phase evolution in the BOF slag systems was predicted via thermodynamic simulations under non-equilibrium cooling conditions, covering a temperature range from 1650 °C to 300 °C. The simulations, based on the Scheil–Gulliver cooling model, are illustrated in Figures 10 (a) to (d). The results indicate that all slag systems (1A, 1D, 3A, and 3D) remain fully liquid at the converter operating temperature of 1650 °C.

For slag samples 1A and 1D, the Scheil–Gulliver cooling predictions indicate that the initial precipitates in both systems consist of a monoxide phase (Ms), composed of (FeO+MnO+CaO+Al2O3+MgO) co-precipitating with a (CaO)2SiO2-(CaO)3P. At lower temperatures, the final predicted phase assemblage includes Spinel (Sp), Monoxide (Ms), Bredigite (B) of (Ca7Mg (SiO4)4 and Brownmillerite Ca2(Al, Fe)2O5.

Samples 3A and 3D exhibit distinct transformation temperatures and a different sequence of phase evolution during cooling compared to the previous slag systems.

However, both slags present the same final phases. Monoxide phase (Ms) which contains the oxides (FeO+Fe2O3+CaO+MgO+Al2O3+MnO) is generated as the first solid precipitate. This precipitate in both cases is combined with α-(CaO)2SiO4. At lower temperatures than ~1532ºC, both systems generate the presence of (CaO)3P which is dissolved at temperatures <1478ºC. Finally, for both slags (3A and 3D) the final phases predicted are Monoxide (Ms), Olivine (O) of (Mg, Fe)2SiO4 and Ca3(Al, Fe)2O6. The four systems at temperatures lower than ~1100ºC are fully solid.

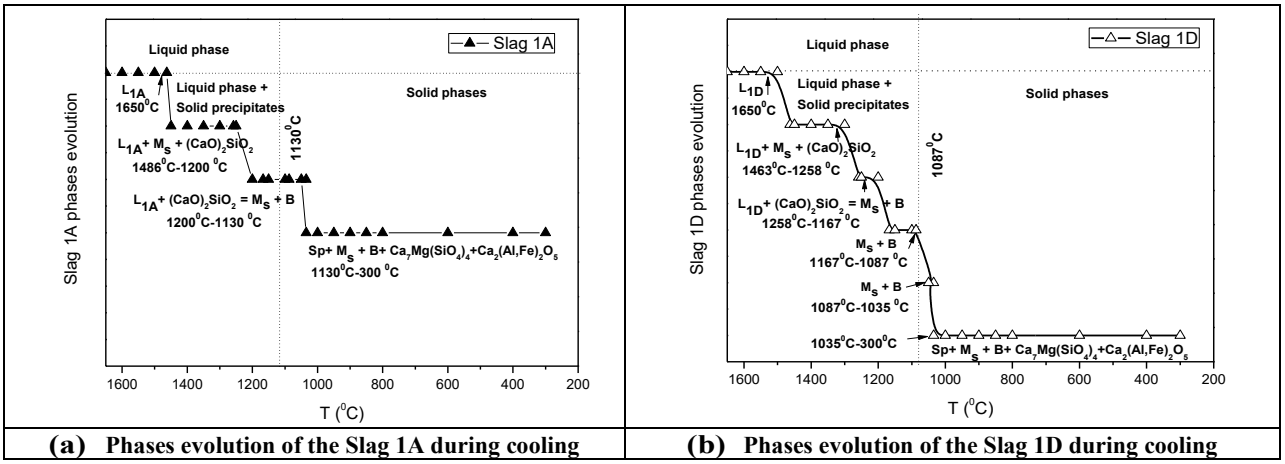

(a) Phases evolution of the Slag 1A during cooling

(b) Phases evolution of the Slag 1D during cooling

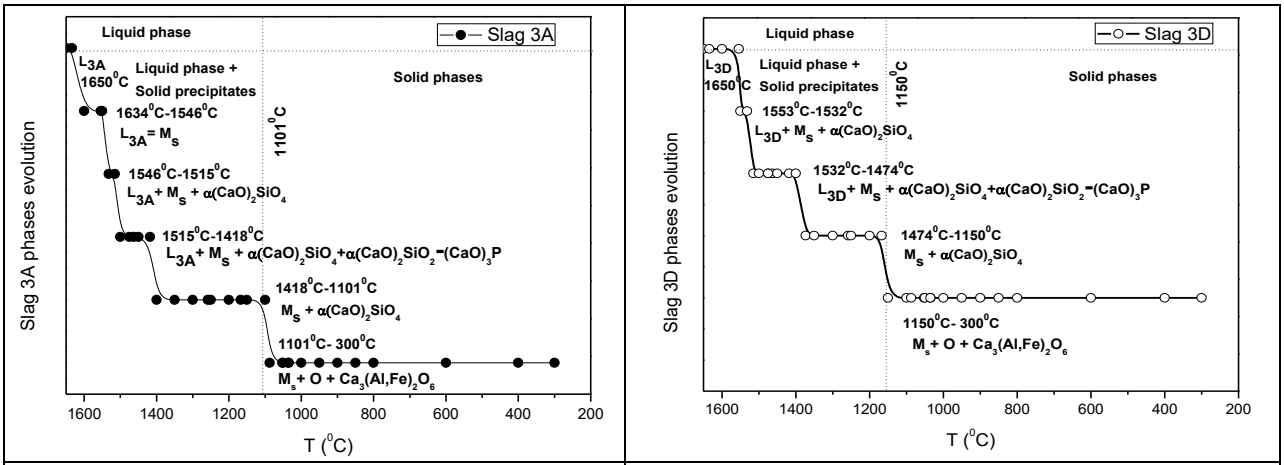

(c) Phases evolution of the Slag 3A during cooling **(d) Phases evolution of the Slag 3D during cooling**

Figure 10: Slag Phases evolution predicted by Scheil-Gulliver cooling model applying Fact Sage

The results of this study confirm that slag foaming is a complex dynamic process where the physical properties and phases evolution of the slag are crucial. The levels and stability of foam determine slag protection efficiency and prevent severe accidents like slopping. The complexity of BOF slag foaming arises because of high temperature, multiphase interactions, and various dynamic factors, making on-site observation and high-temperature studies challenging (Wang *et al.,* 2023). Therefore, slag samples collected at pre- and post-foaming stages provide valuable theoretical and experimental insights. Additionally, thermodynamic simulations under non-equilibrium conditions enhance the understanding of phases systems evolution related to temperature to explain the final phases identified in the slag samples microstructure by microscopy with morphologies (irregular, polygonal, spherical, laminar, and dendritic) within a matrix.

For Samples 1A and 1D, the correlation between thermodynamic predictions and microstructural analysis suggests that the primary final phases are: spinel (Sp), corresponding to the (FG) phase; monoxide (Ms), identified as the dendritic (R) phase; Bredigite (Ca7Mg (SiO4)4) consistent with the (FW) phase; and Ca2(Al, Fe)2O5 which constitutes the (M) matrix.

In Sample 1D, the (Mg, Fe) O monoxide phase is consistent with the irregular (I) morphology, while Ca2(Al, Fe)2O5 appears as a complex assemblage comprising the FP, M, and potentially traces of the L phase. Although various complex spinels were predicted for both systems (1A and 1D), the predominant species is a tetragonal spinel rich in aluminum, calcium, and iron oxides. This finding aligns with the chemical and structural signature of the FG phase identified via SEM-EDS.

The monoxide phase, composed of FeO and MgO, is consistent with the observed (R) phase morphology. The Scheil–Gulliver cooling model effectively describes this phase evolution, including the formation of solid precipitates, based on the assumptions of complete diffusion within the liquid phase, negligible diffusion in the solid state, and local equilibrium at the solid-liquid interface (Chang *et al.,* 2008).

The presence of solid particles significantly influences both the quality and efficiency of slag foaming (Harvey *et al.,* 2020). Thermodynamic modeling further predicts that the liquid-to-solid transformation (solidus temperature) is completed at 1130 °C for Sample 1A and 1035 °C for Sample 1D. Below these temperatures, both slag systems reach a fully solid state. The correlation between basicity (IB2) and physical properties (h and g) indicates that achieving a specific (IB2) range is essential for optimal foaming. This range provides the necessary balance of surface tension and viscosity required to stabilize the slag foam effectively. Within the studied slag systems, the optimal conditions for foaming stability are achieved at a basicity (IB2) of approximately 3.94, a surface tension (g) of 652 mN/m) and a viscosity (h) of 0.6 Poise.

High basicity values (IB2), such as those observed in Samples 1A and 1D, typically require lower contents to reach saturation (see Table 1). In contrast, when (IB2) is approximately 2.0, slag saturation behaves differently, shifting in response to increases in FeO content (Brandaleze *et al.,* 2018).

The slags' melting behavior results (from HSM) indicate that the critical temperatures of post-foaming slags (D) are higher than those of pre-foaming slag samples (A). This is explained through the higher IB2 index values of D slags compared to A, corroborating the dynamic and complex phases evolution during BOF process.

For both bubble sizes, the foaming index (Σ) increases as IB2 decreases, (Table 3). The foam index (S) also is associated with slags FeO contents and it is almost constant for FeO from 20 to 32 % FeO. This is believed to be because above about 25% FeO, the viscosity is

nearly constant (Jung *et al.,* 2000). The slag samples characterized in this study exhibit FeO contents ranging from 23.4% to 31.4%, which are considered appropriate for the BOF process.

The same methodology was applied to Samples 3A and 3D. In comparison to Samples 1A and 1D, these systems exhibit: (a) lower basicity (IB2) values (2.46 and 2.84, respectively), (b) lower surface tension (γ3A= 615 mN/m and γ3D=624 mN/m) and, (c) higher viscosity (h) across the studied temperature range.

Samples 3A and 3D exhibit similar final phase assemblages; however, their morphologies differ significantly from those observed in the other slag samples studied. SEM-EDS analysis reveals a microstructure characterized by a granular matrix, consisting of a complex mixture of the M and SAC phases. The M phase is consistent with the olivine (O) solid solution predicted by the Scheil–Gulliver cooling model. This phase coexists with SAC, a calcium aluminosilicate phase compatible with Ca3(Al, Fe)2O6, which is integrated into the granular matrix of these samples. The identified phases include an irregular grey phase (I), consistent with magnesiowüstite (a common constituent in BOF slags), along with a polygonal precipitate identified as (MW).

Thermodynamic simulations indicate that solid-phase precipitation in Samples 3A and 3D begins at 1634 °C and 1553 °C, respectively. These higher liquidus temperatures compared to Samples 1A and 1D justify the increased viscosity observed in these systems, as the presence of solid precipitates significantly enhances the effective viscosity of the melt (Brandaleze *et al.,* 2018).

When the slag contains sufficient magnesia or reaches MgO saturation, magnesio-wüstite [(Fe, Mg) O] is the first phase to precipitate and crystallize. In Samples 3A and 3D, the (M) phase corresponds to this monoxide solid solution (a complex oxide mixture) while the SAC phase (of Samples 3) consists of calcium silicoaluminate dendrites. The matrix phase is rich in CaO and exhibits a granular morphology, which is consistent with the findings of (Chang K.L. *et al.,* 2008), for BOF slags with low basicity. In Sample 3D, the phases identified during the microstructural study correlate closely with the thermodynamic predictions obtained via FactSage simulations.

Across all slag systems investigated in this study, the observed phase evolution is consistent with the findings reported by (Martinsson *et al.,* 2019). Consistent with the findings of Chang *et al.,* (2008), phosphorus partitioning in high-basicity slags (1A and 1D) occurs within the dicalcium silicate 2CaO.SiO2 phase. In contrast, for low-basicity systems, phosphorus is primarily associated with the kirschsteinite-type CaFeSiO4 phase.

Jung *et al.,* (2000) also confirmed the positive impact of phosphorus associated with silicates, as well as the presence of solid particles (such as dicalcium silicate (2CaOSiO2) or magnesiowüstite ((Fe, Mg) O) on foaming stability. These precipitates increase the bulk viscosity of the slag, thereby promoting foam formation. Furthermore, smaller second-phase particles contribute to stabilizing the foam by retarding film drainage.

A comprehensive understanding of BOF slag behavior is critical not only for optimizing slag foaming and preventing slopping, but also for controlling key metallurgical reactions, such as decarburization and dephosphorization.

Correlating the physical properties behaviour with the evolution of the slag phases, it is possible to think that the slag 3A (pre foaming) could provide a good foaming behaviour justified in the highest viscosity (η) values at process operation conditions combined with a lowest surface tension (γ3A=615 mN/m). The low surface tension favors the formation of small bubbles in the slag and promotes a high foam level without slopping risks (Martinsson *et al.,* 2019). As second alternative could be the slag 1A which exhibits the lowest viscosity values, contains Merwinite (Ca3MgSi2O8) particles that may increase the viscosity of the slag liquid phase. This can reduce bubble film drainage, lower the risk of coalescence, and prevent foam collapse. Thus, slag 1A may be considered a secondary slag suitable for foaming practices.

The integration of the results provided by theoretical models, thermodynamic simulations, and experimental structural studies shows that both slags samples (1A and 3A) are complex phase systems with good foaming capabilities to preserve the refractory lining and that also play significant metallurgical roles in steelmaking, including decarburization, dephosphorization. The methodology of study also provides a valuable information on the BOF slags evolution during operation, associated to the phases mineralogy composition and corroborates that phosphorus is linked to a phase containing CaFeSiO4 or (CaO)2SiO2-(CaO)3P in those with a high basicity index. The Scheil–Gulliver cooling assumptions is considered a good tool to provide complete information associated to the evolution of the slags during cooling from the BOF operation temperatures 1650ºC to 300ºC because the results are consistent with the phases identified experimentally on the slag structure (Durinck D. *et al.,* 2007).

CONCLUSIONS

The evolution of phase composition and mineralogy in BOF slags directly governs their physical properties (viscosity, surface tension) and therefore controls foaming behavior and foam stability. This relationship determines the efficiency of refractory protection during blowing and influences key

metallurgical reactions such as decarburization and dephosphorization.

Non-equilibrium thermodynamic simulations using the Scheil–Gulliver approach (FactSage 8.1, 1650 °C → 300 °C) reproduce the sequence of phase precipitation observed experimentally by SEM–EDS. The close agreement between predicted and observed phases demonstrates that such simulations are a reliable and useful tool to interpret phase evolution and to complement microstructural studies of complex BOF slag systems.

Among the tested slags, sample 3A exhibits the most favorable foaming conditions under the studied operating regime: relatively high melt viscosity combined with lower surface tension results in a high foaming index ($\Sigma \approx 0.265$ for bubble diameter D1 = 0.005 m and $\Sigma \approx 0.098$ for D2 = 0.015 m). These properties favor the formation of small, dense bubbles and a stable foam layer that effectively protects the refractory while minimizing slopping risk.

Thermodynamic prediction and microstructural analysis identify the principal solid constituents in 3A as a monoxide solid solution (Ms, containing Fe–Mg–Ca–Al–Mn oxides), olivine-type silicate (O, (Mg, Fe)2SiO4), and a calcium aluminate/ silicoaluminate phase (Ca3(Al, Fe)2O6, denoted SAC). These solids form a granular matrix and dispersed second-phase particles (I, MW) that raise the effective viscosity and retard film drainage, contributing to foam stabilization.

Slag 1A represents a viable secondary foaming candidate: despite lower bulk viscosity, the presence of solid particles such as merwinite and dicalcium silicate can increase local effective viscosity and impede film drainage, reducing bubble coalescence and preserving foam structure during operation.

The study shows that higher basicity (IB2 = CaO/SiO2) strongly affects surface-layer structure and surface tension through changes in network depolymerization and non-bridging oxygen concentration. Within the analyzed range, basicity and FeO content jointly modulate viscosity and surface tension; controlling these compositional parameters is therefore essential to reach the balanced conditions required for effective foaming.

Solid precipitates (e.g., dicalcium silicate, magnesio-wüstite, spinel-type phases) play a dual beneficial role: they act as interfacial stabilizers at the gas–liquid boundary and increase bulk/effective viscosity, both of which slow film drainage and enhance foam lifetime. Particle size and abundance determine whether this effect promotes stable foam or contributes to undesirable structural changes.

Hot-stage microscopy and modeled viscosity/surface-tension trends confirm that post-foaming slags (samples D) display higher critical temperatures and altered physical-property profiles relative to pre-foaming slags (samples A), reflecting the dynamic compositional and phase changes occurring during blowing.

Operationally, an integrated approach combining compositional control (IB2, FeO, P2O5), thermophysical property estimation, targeted thermodynamic simulation, and microstructural monitoring provides the most robust strategy to optimize slag foaming: maximize refractory protection, maintain process safety (minimize slopping risk), and preserve favorable metallurgical performance.

REFERENCES

- Martinsson J., Glaser D., Sichen D. (2019). The structure of foaming BOF-converter slag, *Ironmaking & Steelmaking, 46*(8),1. https://doi.org/10.1080/03019233.2017.1410950
- Jung S. M., Fruehan R.J. (2000). Foaming Characteristics of BOF Slags, *ISIJ International, 40*(4), 348. https://www.jstage.jst.go.jp/article/isijinternational 1989/40/4/40_4_348/_pdf
- Wang R., Zhang B., Liang Y., Liu C., Jiang M. (2023). Micro insight into foaming behavior of CaO–SiO_2–Fe_xO–MgO-based slag induced by slag/metal reaction, *Ceramics International*, *49*(11), 17185. https://doi.org/10.1016/j.ceramint.2023.02.082
- Brandaleze E., Benavidez E. Santini L. (2018). Treatments and Recycling of Metallurgical Slags, In Recovery and Utilization of Metallurgical Solid Waste (Y. Zhang (ed.)), InTechOpen.
- Skupien D., Gaskell D. R. (2000). The surface tensions and foaming behavior of melts in the system CaO-FeO-SiO_2, *Metallurgical and Materials Transaction B,31*, 921. https://doi.org/10.1007/s11663-000-0068-1
- Kapilashrami A., Lahiri A.K., Görnerup M., Seetharaman S. (2006). Foaming of slags under dynamic conditions, Metallurgical and Materials Transaction B,37, 145. https://doi.org/10.1007/s11663-006-0090-z
- Matsura H. and Fruehan R.J. (2009). Slag Foaming in an Electric Arc Furnace, *ISIJ International, 49*(10), 145. https://doi.org/10.2355/isijinternational.49.1530
- Urbain G. (1982). Viscosity of liquid silica, silicates and alumino-silicates, *Geochimica et Cosmochimica Acta, 46*(6), 1061. https://doi.org/10.1016/0016-7037(82)90059-x
- Zaharia M., Sahajwalla V., Khanna R., Koshy P., O´Kane P. (2009). Carbon/Slag Interactions between Coke/Rubber Blends and EAF Slag at 1

550°C, *ISIJ International, 49*(10), 1513. https://doi.org/10.2355/isijinternational.49.1513

- Zaaiman S., Muire H., Zietsman J.H., (2024). Slag physical property determination: An overview of experimental and computational methods to determine structure, viscosity, electrical conductivity, and thermal conductivity, Southern African Pyrometallurgy, 169.
- Durinck D., Jones P.T., Blanpain B., Wollants P., Mertens G., Elsen J. (2007), Slag solidification modelling using the Scheil-Gulliver assumptions, *Journal of American Ceramic Society,90*(4)*,* 1177. https://doi.org/10.1111/j.1551-2916.2007.01597.x
- Jung S.M. and Fruehan R. J., (2000), Foaming Characteristics of BOF Slags, *ISIJ International, 40*(4), 348. https://doi.org/10.2355/isijinternational.40.348
- Sukenaga S., Higo T., Shibata H., Saito N., Nakashima K., (2015). Effect of CaO/SiO_2 Ratio on Surface Tension of $CaO–SiO_2–Al_2O_3–MgO$ Melts, *ISIJ International*, 55 (6) 1299. http://dx.doi.org/10.2355/isijinternational.55.1299
- Liu C., Zhang R., Meng Y., Wang Z., Jiao S., Jia J. and Min Y., (2021). Mirco-level Insight into the Surface Tension-structure Relationship of Molten $CaO–MgO–SiO_2–Fe_xO–P_2O_5$ Slags, *ISIJ International*, 61 (11), 2765. https://doi.org/10.2355/isijinternational.ISIJINT-2021-236
- Chang K.L., Huang C.T., Huang W.J., Liu Y.C. (2008). Investigations of Microstructure and Phosphorus Distribution in BOF Slag, China Steel Technical Report, 21, 1. https://www.csc.com.tw/csc_c/ts/ena/pdf/no21/01-K.%20L.%20Chang.pdf
- Harvey J.P., Lebreux-Desilets F., Marchand J., Oishi K.A., (2020) Fettouma Bouarab C., Robelin A. E., Gheribi, A.D. Pelton, On the Application of the FactSage Thermochemical Software and Databases in Materials Science and Pyrometallurgy, *Processes 2020*, *8* (1156), 2. https://doi:10.3390/pr8091156